Analytic Gradients for the Electrostatic Embedding QM/MM Model in Periodic Boundary Conditions Using Particle-Mesh Ewald Sums and Electrostatic Potential Fitted Charge Operators

Simone Bonfrate, Nicolas Ferré, Miquel Huix-Rotllant

Analytic gradients for the electrostatic embedding QM/MM in periodic boundary conditions using particle-mesh Ewald sums and electrostatic potential fitted charge operators

Simone Bonfrate, Nicolas Ferré, and Miquel Huix-Rotllant*

Aix-Marseille Univ, CNRS, ICR, Marseille, 13013, France.

E-mail: miquel.huix-rotllant@cnrs.fr

Abstract

Long-range electrostatic effects are fundamental for describing chemical reactivity in the condensed phase. Here, we present the methodology of an efficient quantum mechanical/molecular mechanical (QM/MM) model in periodic boundary conditions (PBC) compatible with QM/MM boundaries at chemical bonds. The method combines electrostatic potential fitted (ESPF) charge operators and electrostatic potentials derived from the smooth particle-mesh Ewald (PME) sum approach. The total energy and its analytic first derivatives with respect to QM, MM and lattice vectors allow QM/MM molecular dynamics (MD) in the most common thermodynamic ensembles. We demonstrate the robustness of the method by performing a QM/MM MD equilibration of methanol in water. We simulate the cis/trans isomerization free energy profiles in water of proline amino acid and a proline-containing oligopeptide, showing a correct description of the reaction barrier. Our PBC-compatible QM/MM model can efficiently be used to study chemical reactivity in condensed phase and enzymatic catalysis.

1 Introduction

Quantum mechanical/molecular mechanical (QM/MM) embedding methods have become a popular method for a cost-effective atomistic description of the reactivity of biomacromolecules.[1] Embedding of all-electron QM methods extends the limitations of classical molecular mechanics force fields (FF), allowing the study of complex reactivity in large systems (for which a full QM description is prohibitive) without the need for new parameterization of each non-standard residue.[2]

An accurate QM/MM model requires a proper representation of the electrostatic interaction between the QM and MM subsystems.[3–5] Depending on the property under study, a finite-sized QM/MM model in the gas phase is sufficient for describing the short-range electrostatic influence on the QM electronic density. However, for computing free energy variations, pair distribution functions, diffusion coefficients, etc. a representation based on periodic boundary conditions (PBC) is necessary. The first PBC-based QM/MM models have been addressed with the introduction of a distance cutoff in the interaction of the original cell with its replicas,[6,7] despite this has been shown to lead to an incomplete description of the long-range electrostatic interactions.[8–15] Alternative methods for improving the long-range description beyond the cutoff scheme comprises switching and smoothing functions,[16–24] charge projection schemes,[25] Fast Multipole Methods (FMM),[26–28] Ewald sum[29] and related lattice summation methods that reduce the $\mathcal{O}(N^2)$ scaling like particle-particle particle-mesh

(P3M),[27,30,31] particle mesh Ewald (PME),[32,33] and others.[34–36] Additional strategies involve hybrid techniques,[13,37–40] which combine explicit modeling of the short-range environment with continuum solvation methods.[41,42]

The Ewald sums method is one of the most popular methods for handling long-range interactions.[29] The total electrostatics converges faster when the interaction is split into the fast (slowly) converging short (long)–range terms computed in the real (reciprocal) space. One of the first Ewald formulations of PBC-adapted QM/MM was proposed by York and coworkers, which relies on semi-empirical methods to describe the QM region.[43] In their model, the quantum density in the replicas is represented using Mulliken point charges, and the electrostatic interaction employs the Ewald pair potential. Most of the time, subsequent PBC-ready QM/MM approaches are variations of this first model, and can be classified according to the level of theory used to describe the QM region (i.e., semi-empirical[43–49] or *ab initio*[50–59]), the partial charges used to represent the QM density in the replicas (Mulliken,[43–48,55] electrostatic potential fitted (ESP),[49] charges from electrostatic potentials using a grid-based method (CHelGP),[53,54,57] and others[58,59]) and the Ewald algorithm used to compute the long-range interactions (i.e., standard Ewald,[44,51,52,58] Ewald pair-potential,[43,49,53–55] or PME[45–48,56,59,60]). While analytical gradients are largely available for almost all the semi-empirical based methods, they are scarce for *ab initio* models. To the best of our knowledge, only five *ab initio* QM/MM PBC methods report the expressions for the analytical gradient.[51,55–58]

In a recent paper,[60] we have proposed a new, simple, yet efficient electrostatic embedding PBC-adapted QM/MM model that combines the efficiency of smooth Particle Mesh Ewald (sPME)[33] (state-of-the-art algorithm for the computation of long-range electrostatic interactions) and of the advantages of Electrostatic Potential Fitted (ESPF) charge operators[61,62] to approximately represent the QM density in replicas. Here, we summarize the energy expressions and derive analytic expressions for the energy gradients with respect to the coordinates of the QM, MM atoms, and lattice parameters, necessary to perform molecular dynamics simulations at the QM/MM level in microcanonical, canonical, and isothermal-isobaric ensembles. We show the expressions in the case of covalently bonded QM-MM regions. The validity of our approach, as well as its efficiency, are demonstrated by performing QM/MM MD for methanol in water, and proline aminoacid and oligopeptide in water.

2 Methodology

In a general QM/MM model, the full molecular system is carefully divided into small and large subsystems. The smallest is usually described with a quantum mechanical (QM) approach, comprising two charge densities: the nuclear one approximated with N_{QM} point charges Z_A, and the electronic one represented in an atomic basis set as a density matrix $\mathbf{P}$. The largest subsystem is modeled at the MM level, using FF built upon connected point masses and N_{MM} point permanent multipoles (for the sake of simplicity, only charges are considered hereafter). In the following, we make use of the A (resp. i) index for looping over the QM (resp. MM) centers. The addition of the QM and MM subsystems as well as their interactions results in a QM/MM hybrid model. In the PBC-adapted QM/MM approach described in the following sections, we use a point charge representation of the quantum density in the replica cells.[60] This description can be considered valid when these QM-derived charges are sufficiently far away from the QM density and screened by the rest of the MM charges.[53,54,57]

2.1 Electrostatic potential fitted method

Here, we employ the electrostatic potential fitted (ESPF) method to describe the electrostatic interaction between the QM and MM subsystems. For completeness, we recall the main equations defining the ESPF charge operator,[62] and the energy in the QM/MM PBC frame-

work.[60] We then show the expression for the analytic gradients of the total QM/MM energy. The ESPF charge operator matrix elements (in a given basis set) are obtained as solutions of the following set of linear equations,

$$\sum_{A}^{N_{\rm QM}} \frac{Q'_{A,\mu\nu}}{|\mathbf{r}_k - \mathbf{r}_A|} = V_{k,\mu\nu}\,, \tag{1}$$

where the electrostatic integrals on a grid point k are defined as $V_{k,\mu\nu} = \int d^3\mathbf{r}\ \chi^*_\mu(\mathbf{r})|\mathbf{r}-\mathbf{r}_k|^{-1}\chi_\nu(\mathbf{r})$, in which the positions $\mathbf{r}_k$ are the point coordinates of a Lebedev atom-centered grid defined around the molecule (excluding the van der Waals spheres around atoms), and χ_μ are the atomic basis functions.[61,62] A correction is added to the charge operator matrix elements to ensure the conservation of the total charge and the charge derivatives of the QM subsystem,[62]

$$Q_{A,\mu\nu} = Q'_{A,\mu\nu} - \frac{1}{N_{\rm QM}} \sum_{B}^{N_{\rm QM}} \left(Q'_{B,\mu\nu} - S_{\mu\nu}\right), \tag{2}$$

in which $S_{\mu\nu} = \int d^3\mathbf{r}\ \chi^*_\mu(\mathbf{r})\chi_\nu(\mathbf{r})$ denotes an overlap integral and $N_{\rm QM}$ is the number of QM centers. These corrected operators are used to construct the interaction Hamiltonian (vide infra) and the ESPF partial charges centered on the QM nuclei as

$$q_A = Z_A - {\rm Tr}[\mathbf{P}\mathbf{Q}_A]\,, \tag{3}$$

where Z_A is the nuclear charge and $\mathbf{P}$ is the density matrix. It is easy to verify that $\sum_A^{N_{\rm QM}} q_A$ is the total charge of the QM fragment and the sum of partial charge derivatives vanishes.[62]

2.2 Energy

The total energy of the total QM/MM system takes the usual form,

$$E = E_{\rm QM} + E_{\rm MM} + E_{\rm int}\,, \tag{4}$$

in which $E_{\rm QM}$ is the energy part from the gas phase Fock operator, $E_{\rm MM}$ encompass the MM FF energy and vdW interactions between the QM and MM subsystems as well, while $E_{\rm int}$ contains all the electrostatic interaction terms between the two subsystems. The definition of the interaction energy in the case of PBC-adapted QM/MM employing ESPF charges was defined elsewhere.[60] The PBC-adapted electrostatic interaction energy between the QM and MM subsystems can be written in simple terms from electrostatic potentials as

$$E_{\rm int} = \sum_{A}^{N_{\rm QM}} q_A \left(\Phi^{MM}_A + \frac{1}{2}\Phi^{\rm QM}_A\right). \tag{5}$$

The ESPF charges q_A interact with two external potentials: $\Phi^{\rm MM}$ originating from all the permanent MM point charges and $\Phi^{\rm QM}$ originating from the ESPF point charges located in the images of the original cell (replica cells). Deriving E_{int} with respect to the density matrix results in a compact form of the interaction Hamiltonian,

$$h^{\rm ESPF}_{\mu\nu} = -\sum_{A}^{N_{\rm QM}} Q_{A,\mu\nu}\left(\Phi^{\rm MM}_A + \Phi^{\rm QM}_A\right), \tag{6}$$

to be added in the gas phase Fock operator of the QM subsystem. Using standard Ewald sums, the QM and MM electrostatic potentials have the following expressions. The MM potential is

$$\Phi^{\rm MM}_A = \sum_{\mathbf{n}=\mathbf{0}} \sum_{i=1}^{N_{\rm MM}} \frac{q_i}{|\mathbf{r}_{Ai\mathbf{n}}|}{\rm erfc}\left(\beta\,|\mathbf{r}_{Ai\mathbf{n}}|\right) + \frac{1}{\pi V}\sum_{\mathbf{m}\neq\mathbf{0}} \frac{e^{-\frac{\pi^2\mathbf{m}^2}{\beta^2}}}{\mathbf{m}^2}\,{\rm Re}\left[e^{-2\pi i\mathbf{m}\cdot\mathbf{r}_A} S_{\rm MM}(\mathbf{m})\right], \tag{7}$$

in which V is the volume of the cell, β is the Ewald range-separation parameters, $N_{\rm MM}$ is the total number of atoms in the MM region, $\mathbf{r}_{Ai\mathbf{n}} = |\mathbf{r}_A - \mathbf{r}_i + \mathbf{n}L|$ is the distance between QM atom A in the original cell and any MM atom i, and $S_{\rm MM}(\mathbf{m})$ is the structure factor (vide infra). The sum $\mathbf{n}$ runs over all the original and replica cells, while the sum $\mathbf{m}$ runs over the reciprocal space vectors.

The QM potential has a similar expression

which is

$$\Phi_A^{\mathrm{QM}} = \sum_{\mathbf{n}\neq\mathbf{0}} \sum_{B=1}^{N_{\mathrm{QM}}} \frac{q_B}{|\mathbf{r}_{AB\mathbf{n}}|} \mathrm{erfc}\left(\beta\,|\mathbf{r}_{AB\mathbf{n}}|\right) + \frac{1}{\pi V} \sum_{\mathbf{m}\neq\mathbf{0}} \frac{e^{-\frac{\pi^2\mathbf{m}^2}{\beta^2}}}{\mathbf{m}^2} \mathrm{Re}\left[e^{-2\pi i\mathbf{m}\cdot\mathbf{r}_A} S_{\mathrm{QM}}(\mathbf{m})\right] - \frac{2\beta}{\sqrt{\pi}} q_A - \sum_{B=1}^{N_{\mathrm{QM}}}{}' \frac{q_B}{|\mathbf{r}_{AB\mathbf{0}}|} \mathrm{erf}\left(\beta\,|\mathbf{r}_{AB\mathbf{0}}|\right) . \tag{8}$$

The last two terms in Eq. 8 arise to correct respectively for the spurious self-interaction and the double-counting of long-range QM-QM interactions in the original cell.[60] In the previous equations, the structure factors $\mathrm{S_{QM}}$ and $\mathrm{S_{MM}}$ are given by

$$S_{\mathrm{QM}}(\mathbf{m}) = \sum_{A}^{N_{\mathrm{QM}}} q_A e^{2\pi i\mathbf{m}\mathbf{r}_A}$$
$$S_{\mathrm{MM}}(\mathbf{m}) = \sum_{i}^{N_{\mathrm{MM}}} q_i e^{2\pi i\mathbf{m}\mathbf{r}_i} . \tag{9}$$

In practice, the long-range part of the MM and QM potentials (i.e., the second term in Eqs. 7 and 8) is computed using the sPME algorithm proposed by Pedersen and coworkers.[33] To do so, the QM atomic charges are projected on the sPME grid together with the MM atomic charges and used to construct the total long-range potential, Φ_A^{long} which corresponds to the sum of the long-range QM and MM contributions to the potential. The correction arising from the long-range QM-QM interactions in the original cell (i.e., the last term in Eq. 8) is then added *a posteriori* as a correction term. Following this approach, it is possible to apply the original sPME algorithm without introducing any modification.

2.3 Analytic energy gradient

The derivative of the total QM/MM energy (Eq. 4) with respect to any parameter x is given by $d^xE = d^xE_{\mathrm{QM}} + d^xE_{\mathrm{MM}} + d^xE_{int}$. Hereafter, we use the shorthand notation for derivatives as a superscript, which represents a partial derivative ($\partial^xE = \partial E/\partial x$) or a total derivative ($d^xE = dE/dx$). Both derivatives are expressed as E^x if there is no need to specify the type of derivative. The expression for the d^xE_{QM}, that is, the gas phase QM energy, depends on the methodology used, but for most common electronic structure methods, there exist analytic formulas for computing it.[63] Similarly, the d^xE_{MM} contains classical terms with simple analytic formulas for the computation of gradients. Therefore, here we focus on the derivative of the QM/MM interaction energy. In the following, firstly, we discuss the derivatives of the ESPF atomic charges, a quantity that is important for all further development. Then, we detail the computation of the interaction energy partial derivatives with respect to QM and MM centers. In the last part, we describe also the partial derivatives with respect to the lattice parameters, necessary to compute for example the pressure.[64]

The derivation of the interaction energy with respect to a generic atom (i.e., QM or MM) is reported in detail in SI Section 1. If we consider a QM atom B, the derivative can be written as

$$E_{int}^{x_B} = -\sum_{A}^{N_{\mathrm{QM}}} q_A^{x_B} \left(\Phi_A^{MM} + \Phi_A^{\mathrm{QM}}\right) + \sum_{A}^{N_{\mathrm{QM}}} q_A \left(\Phi_A^{MM,x_B} + \frac{1}{2}\Phi_A^{QM,(x_B)}\right) . \tag{10}$$

where the first term contains the derivative of the ESPF charges and the QM and MM Ewald potentials defined in Eqs. 7 and 8. The second term requires, instead, the derivatives of the Ewald potentials with respect to a QM atom coordinate. In the following, we give explicit expressions for constructing the derivative of the total energy.

2.3.1 Atomic charge derivatives

Here, we focus on the construction of the first term of Eq. 10. As the ESPF charges are polarizable, it is possible to write derivatives with respect to a QM coordinate x_B,[65] that are de-

noted as

$$q_A^{x_B} = -\mathrm{Tr}\left[\mathbf{P}\mathbf{Q}_A^{x_B}\right] - \mathrm{Tr}\left[\mathbf{P}^{x_B}\mathbf{Q}_A\right] . \quad (11)$$

A common trick when computing the derivative of the total energy of the system for self-consistent field densities, is that the energy derivative corresponding to the second term of Eq. 11 together with all other terms proportional to the density matrix derivatives in the Fock operator can be substituted for a term containing the derivative of the atomic overlap matrix ($-\mathrm{Tr}\left[\mathbf{W}\mathbf{S}^{x_B}\right]$),[66] where $\mathbf{W}$ is the so-called energy-weighted density matrix and $\mathbf{S}^{x_B}$ is the geometrical derivative of the overlap matrix. Therefore, hereafter we consider only the derivative of the ESPF charges at fixed density,

$$q_A^{x_B} = -\mathrm{Tr}\left[\mathbf{P}\mathbf{Q}_A^{x_B}\right] , \quad (12)$$

where $Q_{A,\mu\nu}^{x_B}$ is the ESPF charge operator derivative which only depends on the coordinates of the QM atoms.

In practice, Eq. 12 is constructed by tracing the density matrix with the operator derivatives expressed as

$$\mathbf{Q}_A^{x_B} = (\mathbf{T}^\dagger\mathbf{T})^{-1}\mathbf{T}^\dagger\left[\mathbf{V}^{x_B} - \mathbf{T}^{x_B}\mathbf{Q}_A\right] , \quad (13)$$

where $\mathbf{T}$ is the electrostatic kernel whose elements are $\mathbf{T}_{k,A} = |\mathbf{r}_k - \mathbf{r}_A|^{-1}$, and $(\mathbf{T}^\dagger\mathbf{T})^{-1}\mathbf{T}^\dagger$ is the pseudoinverse of $\mathbf{T}$.[62]

It follows that, by construction, the derivatives of the ESPF charge operator with respect to the coordinates of MM atoms are always zero. In the rest of the paper, the notation for the superscript derivatives indicates a derivative at fixed density matrix, while the notation for the superscript derivatives in round brackets indicates a derivative at fixed QM charges ($q_A^{(x_B)} = 0$ for any A and B).

2.3.2 External potential derivatives

Here, we focus on the construction of the second term of Eq. 10, when the derivatives concern the coordinates of a QM and MM center, requiring the derivative of the QM and MM external potentials.

The general expression of the QM potential on QM atom center A derivative with respect to the coordinate of QM atom B is given by

$$\Phi_A^{QM,(x_B)} = -{\sum_{B=1}^{N_{\mathrm{QM}}}}' q_B\, d^{x_B}\left(\frac{1}{|\mathbf{r}_{AB\mathbf{0}}|}\right) \quad (14)$$
$$+ \sum_{\mathbf{n}=0}{\sum_{B=1}^{N_{\mathrm{QM}}}}' q_B\, d^{x_B}\left[\frac{\mathrm{erfc}\left(\beta\,|\mathbf{r}_{AB\mathbf{n}}|\right)}{|\mathbf{r}_{AB\mathbf{n}}|}\right]$$
$$+ \frac{1}{\pi V}\sum_{\mathbf{m}\neq 0}\frac{e^{-\frac{\pi^2\mathbf{m}^2}{\beta^2}}}{\mathbf{m}^2}\, d^{(x_B)}\left\{\mathrm{Re}[e^{-2\pi i\mathbf{m}\cdot\mathbf{r}_A}S_{\mathrm{QM}}(\mathbf{m})]\right\} .$$

Similar expressions for the MM potential derivative, as well as developed expressions for both derivatives, can be found in SI Sections 2.1 and 2.2.

The derivatives of QM potentials with respect to MM displacements are zero since the potential only depends on QM coordinates. Therefore, the first derivative with respect to an MM atom coordinate x_i reduces to

$$E_{int}^{x_i} = \sum_{A}^{N_{\mathrm{QM}}} q_A\Phi_A^{\mathrm{MM},x_i} , \quad (15)$$

where the derivative of the MM potential on center A with respect to an MM atom i, is given by,

$$\Phi_A^{\mathrm{MM},x_i} = \sum_{\mathbf{n}=\mathbf{0}}\sum_{i=1}^{N_{\mathrm{MM}}} q_i\, d^{x_i}\left[\frac{\mathrm{erfc}\left(\beta\,|\mathbf{r}_{Ai\mathbf{n}}|\right)}{|\mathbf{r}_{Ai\mathbf{n}}|}\right] \quad (16)$$
$$+ \frac{1}{\pi V}\sum_{\mathbf{m}\neq\mathbf{0}}\frac{e^{-\frac{\pi^2\mathbf{m}^2}{\beta^2}}}{\mathbf{m}^2}\, d^{x_i}\left\{\mathrm{Re}\left[e^{-2\pi i\mathbf{m}\cdot\mathbf{r}_A}S_{\mathrm{MM}}(\mathbf{m})\right]\right\} .$$

The fully developed expression can be found in SI Section 2.1.

From a practical point of view, the derivatives of the long-range part of the potentials (i.e., the last term in Eqs. 14 and 16) are computed using the sPME algorithm, by following the same procedure described for the potential in Section 2.2. Also in this case it is not necessary to modify the original sPME algorithm.

2.3.3 Lattice vector derivatives

The coordinate transformation $\mathbf{r} = \mathbf{hu}$ transforms fractional ($\mathbf{u}$) into Cartesian coordinates ($\mathbf{r}$) through the cell tensor $\mathbf{h}$, which is defined by its transpose as

$$\mathbf{h}^{\mathrm{T}} = \begin{pmatrix} a & b\cdot\cos(\gamma) & c\cdot\cos(\beta) \\ 0 & b\cdot\sin(\gamma) & -c\cdot\sin(\beta)\cdot\cos(\alpha^*) \\ 0 & 0 & c\cdot\sin(\beta)\cdot\sin(\alpha^*) \end{pmatrix}, \tag{17}$$

where a, b and c are the lattice vector lengths, α, β and γ the lattice angles. The superscript * denotes the reciprocal lattice angles, which are related to the real lattice angles through the relation,

$$\cos(\alpha^*) = \frac{\cos(\beta)\cos(\gamma) - \cos(\alpha)}{\sin(\beta)\sin(\gamma)}\,. \tag{18}$$

The total derivatives of the QM/MM energy (Eq. 4) with respect to a lattice parameter a is given by $d^aE = d^aE_{\mathrm{QM}} + d^aE_{\mathrm{MM}} + d^aE_{int}$. The total derivative concerning lattice parameters can be written as the

$$d^aE = \partial^aE + \sum_p^{\mathrm{N}} (\partial^pE)\cdot(\partial^a\mathbf{hu}_p)\,. \tag{19}$$

The first term vanishes for interactions accounted for only in the original cell, namely, the E_{QM} and classical bonded terms in E_{MM}. The second term depends on the derivative of the total energy with respect to the QM or MM coordinates, as already defined in the previous sections, and the derivatives of the atom Cartesian coordinates, with trivial expressions (see Section 4.3 of SI).

The partial derivative of the QM/MM interaction energy can be written as,

$$\partial^aE_{int} = \sum_{A=1}^{N_{\mathrm{QM}}} q_A\left(\Phi_A^{MM,a} + \frac{1}{2}\Phi_A^{QM,a}\right) \tag{20}$$

The only term within Φ_A^{QM} that has non-zero derivatives with respect to the lattice parameters is the long-range potential in the reciprocal space (second term in Eq. 8), containing an explicit dependence on the volume of the simulation cell. Considering a cubic box, the derivatives with respect to cell length are written as

$$\Phi_A^{QM,a} = -\frac{3a^2}{\pi V^2}\sum_{\mathbf{m}\neq 0}\frac{e^{-\frac{\pi^2\mathbf{m}^2}{\beta^2}}}{\mathbf{m}^2}\,\mathrm{Re}\left[e^{-2\pi i\mathbf{m}\cdot\mathbf{r}_A}S_{\mathrm{QM}}(\mathbf{m})\right] \tag{21}$$

while the derivatives with respect to cell angles are equal to zero, as the volume in the cubic cell is expressed as $V = a^3$. A more general expression could be found in Section 4 of the SI.

2.4 Bonded QM-MM boundaries

Covalent bonds between the QM and MM regions create an unsaturated QM atom that fictitiously overpolarizes the QM density. Many methods exist to solve this problem.[67–85] The link atom (LA) remains the simplest and most widely used approach,[86–88] in which a QM auxiliary atom is placed between the QM and MM frontier atoms. According to Morokuma's scheme,[89] a LA is placed onto each QM and MM frontier (f),

$$\mathbf{r}_f = \mathbf{r}_{f,\mathrm{QM}} + g_f(\mathbf{r}_{f,\mathrm{MM}} - \mathbf{r}_{f,\mathrm{QM}})\,, \tag{22}$$

in which $\mathbf{r}_f$, $\mathbf{r}_{f,\mathrm{QM}}$ and $\mathbf{r}_{f,\mathrm{MM}}$ are respectively the positions of the LA, QM, and MM frontier atoms. Therefore, the index f labels both the LA and the corresponding QM–MM frontier bond. The factor g_f has a fixed value depending only on the nature of the QM and MM frontier atoms. For example, in a frontier bond between two carbon atoms, the LA is usually taken as a hydrogen atom, and g_f is taken as the ratio between the standard covalent bond lengths of a C−H and a C−C bonds.

Since LAs have basis functions centered on their nuclei, the QM electron density can extend onto them. Accordingly, each LA holds a partial atomic charge that saturates the valency of the corresponding frontier QM atom. Therefore, LAs enter in the definition of the QM/MM

interaction energy

$$E_{int} = \sum_{A}^{N_{\rm QM}} q_A \left(\Phi_A^{MM} + \frac{1}{2}\Phi_A^{CQ} \right) + \sum_{f}^{N_{\rm LA}} q_f \left(\Phi_f^{MM} + \frac{1}{2}\Phi_f^{CQ} \right), \quad (23)$$

in which $N_{\rm LA}$ is the number of LAs and CQ = QM + LA. The atomic partial charges $q_A = Z_A - Q_A$ ($q_f = Z_f - Q_f$) are computed as the difference between the nuclear charge and the net electronic population. The construction of the interaction energy requires the CQ potential, which is essentially the same potential as defined in Eq. 8 with the addition of the interaction of QM atoms with frontier atoms (see Section 3 of SI).

In Morokuma's original proposal,[89] the LA contributions to the total energy gradient with respect to nuclear coordinates are projected back to the frontier atoms to retrieve the correct dimensionality of the potential energy surface,

$$\frac{dE}{d\mathbf{r}_{f,\rm QM}} = \frac{\partial E}{\partial \mathbf{r}_{f,\rm QM}} + (1-g_f)\frac{\partial E}{\partial \mathbf{r}_f}$$
$$\frac{dE}{d\mathbf{r}_{f,\rm MM}} = \frac{\partial E}{\partial \mathbf{r}_{f,\rm MM}} + g_f \frac{\partial E}{\partial \mathbf{r}_f}. \quad (24)$$

This requires thus the derivative of the link atom energy expression (Eq. 23). Explicit expressions for these derivatives are similar to those in Eqs. 16 and 14 and can be found in the SI.

A non-neutral cell might be formed when cutting a frontier between QM and MM, i.e., $Q_{CQ} + Q_{\rm MM} = Q_{tot} \neq 0$, where $Q_{CQ} = \sum_A^{N_{\rm QM}} q_A + \sum_f^{N_{LA}} q_f$ and $Q_{\rm MM} = \sum_i^{MM} q_i$. This is because the QM subsystem is enforced to have an integer charge, whereas the MM subsystem does not. To guarantee the correct system's total charge, we apply an *a posteriori* extra-correction to the QM atomic charges $q_A = q'_A + q^{corr}$, where

$$q^{corr} = \frac{Q_{tot} - Q_{\rm CQ} - Q_{\rm MM}}{N_{\rm CQ}} = \frac{Q_{corr}}{N_{\rm CQ}}, \quad (25)$$

We use these charges in the definition of energy and derivative. The energy (Eq. 10) is then given by

$$E_{int} = E'_{int} + Q_{corr}\left(\Phi_{av}^{MM} + \Phi_{av}^{CQ} + \frac{1}{2}\Phi_{av}^{corr} \right), \quad (26)$$

where the average potentials Φ_{av}^{CQ}, Φ_{av}^{MM} and Φ_{av}^{corr}, generated respectively by the replicas of QM and LA charges, by MM charges, and by the charge correction, can be defined as

$$\Phi_{av}^{MM} = \frac{1}{N_{\rm CQ}} \sum_{\alpha=1}^{N_{\rm CQ}} \Phi_\alpha{}^{MM}, \quad (27)$$
$$\Phi_{av}^{QC} = \frac{1}{N_{\rm CQ}} \sum_{\alpha=1}^{N_{\rm CQ}} \Phi_\alpha{}^{CQ},$$
$$\Phi_{av}^{corr} = \frac{Q_{corr}}{N_{\rm CQ}^2} \sum_{\alpha,\gamma=1}^{N_{CQ}} \phi_{\alpha\gamma}.$$

In the previous equations, α and γ indicate any QM or LA atoms, and $\phi_{\alpha\gamma}$ is the Ewald pair potential between two atoms, whose definition can be found in Section 5 of SI.

Since the values Q_{tot}, Q_{CQ} and $Q_{\rm MM}$ are fixed parameters, any derivative of q_A is equal to the derivative of the uncorrected q'_A. Therefore, the charge-derivative term of Eq. 10 remains the same, and so the corrected derivatives are

$$E_{int}^{x_B} = E_{int}^{',x_B} + Q_{corr}\left(\Phi_{av}^{CQ,x_B} + \Phi_{av}^{corr,x_B} \right)$$
$$E_{int}^{x_i} = E_{int}^{',x_i} + Q_{corr}\Phi_{av}^{MM,x_i}, \quad (28)$$

in which the average potential derivatives are given by

$$\Phi_{av}^{MM,xi} = \frac{1}{N_{CQ}} \sum_{\alpha=1}^{N_{CQ}} \Phi_\alpha^{MM,x_i}, \quad (29)$$
$$\Phi_{av}^{CQ,x_B} = \frac{1}{N_{CQ}} \sum_{\alpha=1}^{N_{CQ}} \left(\Phi_\alpha^{CQ,(x_B)} + \sum_{\gamma=1}^{N_{CQ}} q_\gamma^{x_B}\phi_{\alpha\gamma} \right),$$
$$\Phi_{av}^{corr,x_B} = Q_{corr}\frac{1}{N_{CQ}^2} \sum_{\alpha,\gamma=1}^{N_{CQ}} \phi_{\alpha\gamma}^{x_B}.$$

3 Computational details

The described electrostatic embedding PBC-adapted QM/MM analytic gradients have been implemented for restricted, unrestricted, and restricted open-shell single-determinant self-consistent fields (SCF) (i.e., Hartree-Fock, HF, or density-functional theory, DFT) in a development version of GAMESS-US (2021R) interfaced with TINKER 8.10.1. The implementation of the energy is detailed in Ref. 60. In summary, the QM part of the external potential depends on the QM density via the partial QM charges of the replicas (see Eq. 8). This implies that, at every SCF step, a new external potential is generated and included in the one-electron Hamiltonian until convergence. The long-range part of the potential is computed using the standard sPME algorithm as implemented in TINKER,[33] from which we extract the external potential at the position of the QM (and, if required, LA) centers. Upon convergence of the QM density, the final set of QM charges is extracted and the final classical electrostatic and the rest of MM interactions are added, leading to the full energy of the system (Eq. 4).

Ewald sPME was used to compute electrostatics in all the systems studied below. The range separation value β was chosen in each system so that the contributions to the real-space potential arising from charges outside the chosen cutoff radius are less than a threshold value of 10^{-8} kcal·mol^{-1}. The 5th-order B-splines and tinfoil boundary conditions were used for each studied system. In all the QM/MM calculations an SCF convergence threshold of 10^{-6} Hartree has been used. In each MD simulation, an additional correction of the velocities has been applied at each integration step to enforce the translational and rotational invariance of the center of mass of the system. Free energy profiles have been reconstructed from umbrella sampling (US),[90] data by applying the weighted histogram analysis method (WHAM) algorithm,[91] using the code provided by Grossfield.[92] The image structures of proline and proline-containing peptide systems have been generated using the UCSF ChimeraX molecular visualization tool.[93] Additional details about the protocols employed for the QM/MM MD equilibration and for the US calculations can be found in Section 6 of SI.

4 Results and discussion

4.1 QM/MM molecular dynamics

For validating our implementation, we performed geometry optimization, and the NVE, NVT, and NPT MD at the QM/MM level for a test system of methanol in water, (see Fig. 1). The chosen level of theory was HF/6-31G*//CHARMM22.[94,95] These are all the necessary steps to prepare a system for production, from relaxation to equilibration in main thermodynamical ensembles. In the following, we discuss the results independently for each equilibration step.

4.1.1 Geometry optimization

The QM/MM energy minimization using micro iterations was performed until the maximum gradient was lower than 10^{-4} Hartree·bohr^{-1} and the root mean square (RMS) of the gradients on the QM atoms was lower than $0.5 \cdot 10^{-5}$ Hartree·bohr^{-1}. The microiteration approach implies that, at every QM geometry optimization step (done by GAMESS-US using a quadratically convergent algorithm), the MM environment is minimized at frozen QM coordinates (performed in the TINKER software).[96] In the final optimized structure, the O-H distance is 0.96 Å, the C-O distance is 1.41 Å, and the average C-H distance is 1.08 Å. At the same time, the C-O-H angle has a value of 109.35° while the H-C-H angles have an average value of 108.76 ± 0.35°.

4.1.2 NVT and NPT molecular dynamics

In Fig. 1 (b) and (c) we reported, respectively, the results of subsequent NVT and NPT QM/MM MD equilibrations. The NVT dynamics have been propagated for 250 ps starting

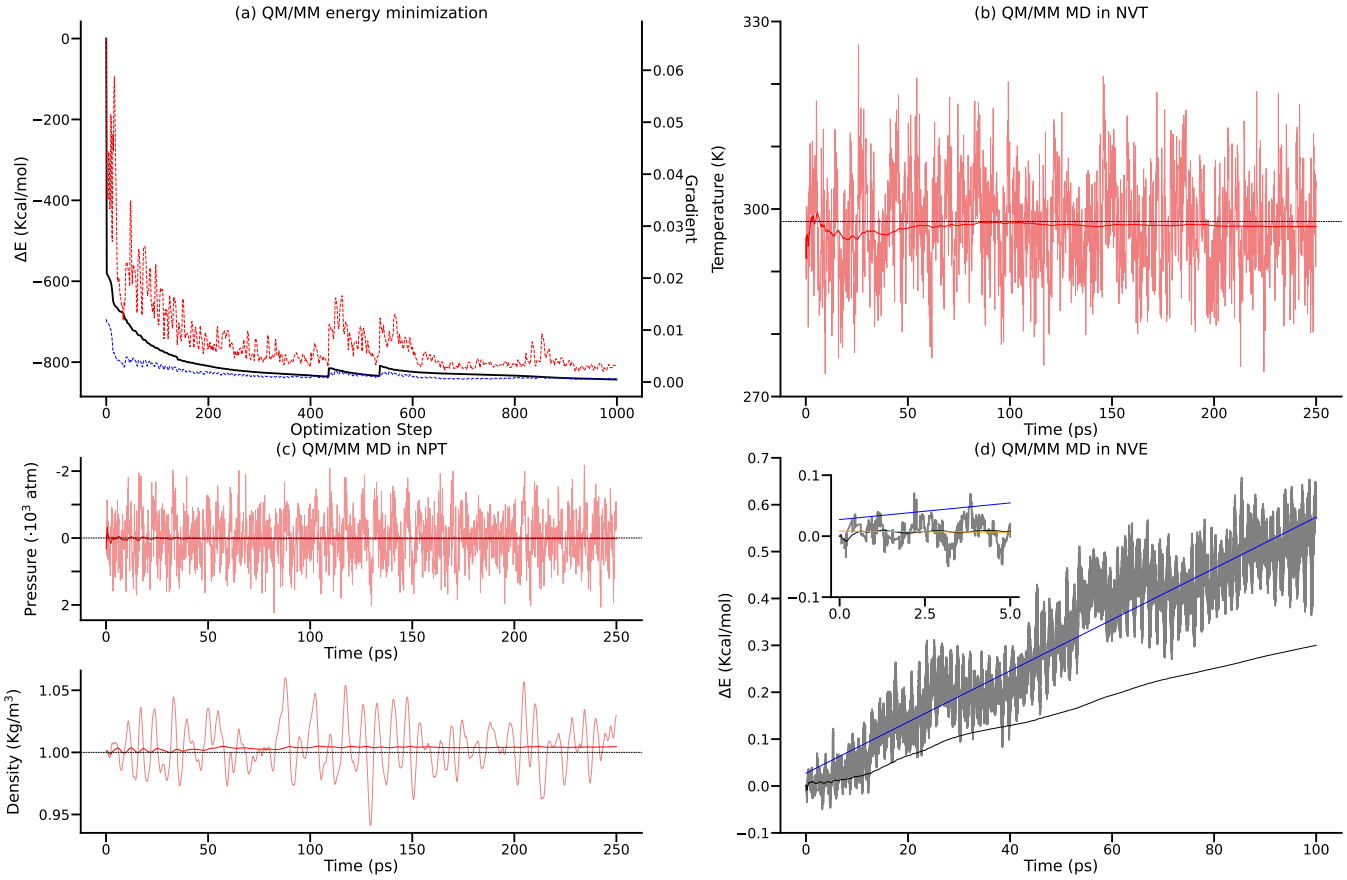

Figure 1: Convergence of the QM/MM equilibration steps performed for the methanol model in water, for (a) QM/MM energy minimization, (b) QM/MM MD in NVT ensemble, (c) QM/MM MD in NPT ensemble. Panel (d) reports the results of QM/MM MD in the NVE ensemble with an inset that shows in more detail the first 5 ps On the left axis, the energy is depicted, shown in the black solid line for the running average and in grey the instantaneous value. Energies are in kcal · mol^{-1} relative to a reference value taken as the t_0 energy value. On the right axis, the convergence criteria are depicted, depending on the equilibration step. For the optimization, the blue and red lines correspond to the absolute maximum and RMS of the gradient in Hartree·$bohr^{-1}$ respectively. For the NVE the blue and orange lines correspond to curves linearly fitted to the energy along the full trajectory and in the first 5 ps respectively. For the NVT, the red line corresponds to the temperature in Kelvin and the NPT to the pressure in atmospheres and density in g·cm^{-3}.

from the system equilibrated at MM level. The system was thermostated at 298 K and we get an average value of the temperature of 297.20 ± 7.77 K. Using the geometry and the velocities of the last NVT step, the trajectory has been propagated further in the NPT ensemble for another 250 ps, with a target pressure of 1 atm. The average value of pressure was -67.98 ± 596.84 atm (almost indistinguishable from the requested value due to the large standard deviation) and the average value of density was 1.00 ± 2.22 · 10^{-16} g · cm^{-3}. The average distances over the 250 ps NVT and NPT trajectory, with snapshots sampled every 100 fs, have values similar to those observed in the optimized structure. In particular, the distances are 1.41 ± 0.04 Å for the C-O, 0.96 ± 0.03 Å for the O-H, and 1.09 ± 0.03 Å for the C-H. Similarly, the average values for the angles along the NVT and NPT trajectory are close to those of the optimized structure. In more detail, the average angles registered during the NVT dynamics are 109.47 ± 4.05° for the C-O-H angle, and 108.46 ± 5.37° for the H-C-H angles, while the values for the same angles along the NPT trajectory are 109.43 ± 3.97° and 108.46 ± 4.55° respectively.

4.1.3 NVE molecular dynamics

A common test usually made to evaluate the quality of an MD implementation consists of testing the energy conservation during a simulation in the microcanonical ensemble (NVE).[97] We assess the capability of our PBC-adapted QM/MM MD method to conserve the total energy we propagated a trajectory for 100 ps starting from optimized geometry and a set of random velocities extracted from a Maxwell-Boltzman distribution at 298 K. On such a time scale, it would be possible to disentangle the effects of systematic errors (i.e., constant errors that are added at each time step and are due to the finite precision used during calculations), causing a linear energy drift in time, from errors from other sources that have a non-linear behavior and can be predominant at shorter time scales.[98] In Fig. 1 (d) we reported the variation in the total energy as a function of time as $\Delta E(t) = E(t) - E(0)$ as well as the total energy running average computed as $\langle E(t) \rangle = (\sum_{i=0}^{t} E_i - E_0)/(t+1)$. A first inspection of such data shows that the total energy presents a mostly linear, upward drift. The drift rate, obtained from the slope of a linear fitting of the total energy, is 5.46 ·10^{-3} kcal·mol^{-1}·ps^{-1} (8.70 ·10^{-6} hartree ·ps^{-1}) results in a total of 5.95 kcal·mol^{-1} gained by the system during the simulation, which accounts for the 7.94·10^{-4} % compared to the average total energy of the system that is -75551.28 ± 0.17 kcal·mol^{-1}. Although very stringent conservation thresholds are usually required in pure MM implementations,[97] looser thresholds are generally considered acceptable for *ab initio* QM/MM approaches.[99]

Similar results have been obtained for a water box of 20 Å side in which one water molecule is described at the QM level. In this case, we observe a drift rate of 1.49 · 10^{-3} kcal·mol^{-1}·ps^{-1} with a total energy variation of 1.81 · 10^{-1} kcal·mol^{-1}, which consist in the 3.52 · 10^{-4} % of the average total energy of the system of -51151.38 ± 0.05 kcal·mol^{-1}, thus further confirming the capability of our method to conserve the energy with an acceptable level of accuracy (see Fig. 2 of SI for more details).

Finally, in the inset of Fig. 1 (d), we zoom in on the first 5 ps of the NVE trajectory. By fitting a linear function to these data, a drift rate of -3.65 · 10^{-4} kcal·mol^{-1}·ps^{-1} is obtained. This underestimation of effective linear drift observed on a longer time scale can be explained by the presence of other sources of error, with non-linear behavior, that on such a short time scale are predominant (e.g., random errors, which have diffusive behavior). These findings suggest that the attempts to predict the trend of the linear component of the drift from short simulations can be inaccurate if the effects arising from the non-linear components are not ruled out.

4.2 Peptidyl-prolyl bond isomerization free energy profile

Proline peptide bond isomerizations are of fundamental importance in the folding of pro-

teins and usually constitute the rate-limiting step,[100,101] catalyzed by peptidyl-prolyl cis-trans isomerases (PPIases) enzymes.[102,103] There exist numerous experimental and computational studies conducted on the isomerization of proline-containing peptides, providing a perfect benchmark of our QM/MM MD methodology.[104–110] Therefore, we applied it to the cis-trans isomerization of peptidyl-prolyl bond first on an analog model system, which is Ace-Pro-NHMe, and then on the succinyl-Ala-Ala-Pro-Phe-p-nitroanilide (AAPF) peptide which is a common substrate for studies of the catalytical activity of cyclophilin enzyme.[106,110]

4.2.1 Proline isomerization in water

In Fig. 2(a), we reproduced the structure of the simulated system, where we treated quantum-mechanically the proline molecule, capped using acetyl and N-methyl amide fragments, while the solvent is described classically using the TIP3P model.[111]

In Fig. 2(b), we report the free energy profiles of proline associated with the isomerization of the peptidyl bond as computed at the HF/3-21G,[112] (depicted in red) and B3LYP/6-31G* (depicted in dark red) levels of theory. For the sake of comparison, we reported also the profiles computed at the MM level of theory, using standard Amber99sb parameters,[113,114] (depicted in light blue) and a modified set of Amber99sb parameters (depicted in blue).[115] In particular, in the modified set, the heights of the barrier associated with the peptidyl bond torsion have been adjusted in order to reproduce the experimental data. For comparison purposes, the zero has been arbitrarily set to the free energy value of the trans isomer.

Compared with the experimental data,[104] the HF profile recovers correctly both the relative energies of the cis and trans isomers as well as the torsional angle and energy of the transition state. On the one hand, the trans-to-cis barrier is slightly underestimated, with a $\Delta\Delta G^{\ddagger}$ of 0.32 kcal·mol^{-1}. On the other hand, the trans/cis free energy difference ($\Delta\Delta G$ = 1.93 kcal·mol^{-1}) is higher than the experimentally reported value. The lower accuracy with respect to the results obtained at the MM level, using the modified set of parameters, can be rationalized by considering the low level of theory employed for the QM/MM calculations.

The profile computed using DFT, instead, recovers the relative energies of the cis and trans isomers correctly but largely underestimates the height of the barrier. This behavior can be explained by the tendency of DFT, due to self-interaction error, to overstabilize delocalized densities that usually characterize the distorted geometries of transition state structures.[116,117]

4.2.2 AAPF peptide isomerization in water

In Fig. 3(a), we reproduced the structure of the simulated system. The succinyl-Ala-Ala-Pro-Phe-p-nitroanilide (AAPF) peptide has been partitioned into two fragments, the first one, which encompasses the proline and one of the alanine residue, is described at the HF/3-21G level of theory (shown in balls and sticks in the figure), while the second one, which contains all the other residues and the cappings, is described at the MM level using Amber99sb and GAFF parameters (shown in lines in the figure).[118] The aforementioned partitioning introduces two frontiers between the QM and MM regions that were handled with two link atoms (shown in magenta in the figure). The solvent is described classically using the TIP3P model.

In Fig. 3(b), we report the free energy profile of the isomerization of the peptidyl bond in the AAPF peptide. In the same figure is reported for comparison, the profile for the same reaction, computed at the MM level of theory using the modified set of Amber99sb parameters (depicted in blue).[115] Again, for the sake of comparison, the zero has been defined to correspond to the free energy value of the trans isomer.

As visible from the figure, we could not compute the free energy profile at the QM/MM level in the interval between 0 and 70 degrees. In such cases, we observed an overpolarization of the quantum density around the frontier region, which is a well-known limitation of the link-atom approach applied to the backbone of

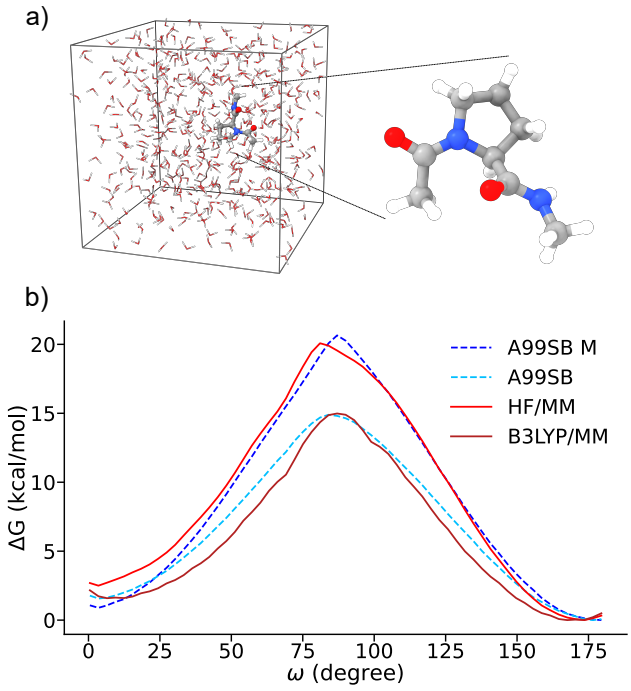

c)

	$\Delta G^{\ddagger}$ (trans → cis)	ΔG (cis-trans)
Exp	20.40	0.57±0.07
A99SB	14.89±0.09	1.57±0.10
A99SB M	20.65±0.08	0.89±0.07
HF/MM	20.08±0.03	2.50±0.04
B3LYP/MM	14.99±0.02	1.59±0.05

Figure 2: (a) Structure of the QM/MM PBC model of proline model system in a water box, with a highlight of the QM region on the right. (b) Isomerization free energy profile for proline, showing the profile obtained using the new QM/MM PBC-adapted model described in this article at HF/3-21G//Amber99sb (labeled HF/MM in red) and at B3LYP/6-31G*//Amber99sb (labeled B3LYP/MM in dark red), as well as the profiles generated using Amber99sb modified (in blue) and unmodified parameters (in light blue). (c) The table shows experimental and computed activation energy as well as the difference in free energy between the cis and trans isomers.

peptides.[119] Consequently, as the experimental data reported in the literature,[120] refer to the cis-to-trans isomerization, a direct comparison with the experiment is currently not possible, as we could not assess the relative free energy of the cis isomer. However, from the comparison with the profile computed at the MM level, which in turn is in good agreement with the experiments, it is possible to see that the *ab initio* calculations correctly reproduce the prediction on the position and height of the trans-to-cis barrier obtained with modified parameters ($\Delta\Delta G^{\ddagger} = 0.17\pm0.08$ kcal·mol^{-1}), thus suggesting that the QM/MM model is appropriate to predict the isomerization behavior.

A further element in support of such claims comes from the comparison with the results obtained at QM/MM for the proline case. Moving from the simple model system to the peptide, we predict an increment of the $\Delta G^{\ddagger}$ of 0.7±0.06 kcal·mol^{-1}, which is coherent with the steric encumbrance generated by the larger substituents in the peptide compared to the lighter cappings in the proline model.

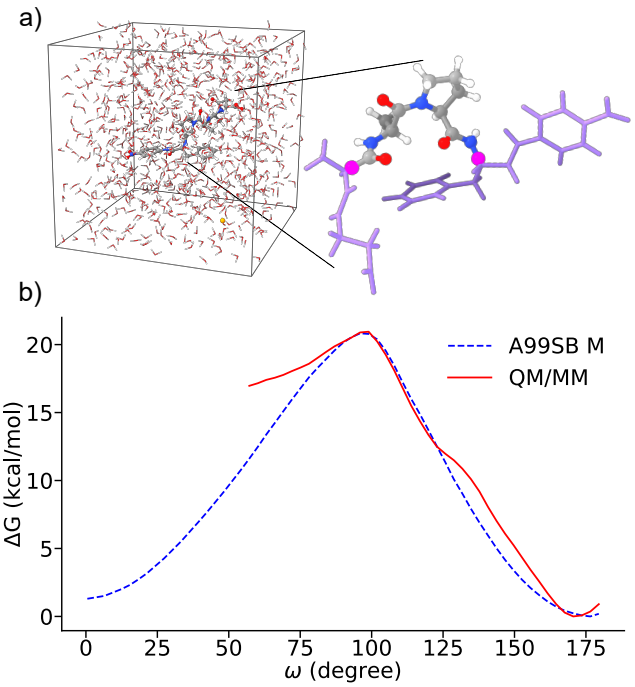

Figure 3: (a) Structure of the QM/MM PBC model of AAPF peptide system in a water box, with a highlight of the peptide on the right. The QM region is shown using balls and sticks representation while the link atoms are shown in magenta. (b) Isomerization free energy profile for the AAPF peptide, showing the profile obtained using the new QM/MM PBC-adapted model described in this article (in red) as well as the profiles generated using Amber99sb modified parameters (in blue).

5 Conclusions

We have derived the analytic energy gradients of periodic boundary condition compatible *ab initio* electrostatic embedding QM/MM method, that combines the strengths and efficiency of electrostatic potential fitted charges and particle-mesh Ewald potentials. We show the expressions for derivatives with respect to all system parameters, namely, the QM and MM atoms and the lattice parameters, allowing molecular dynamics at the QM/MM level in the microcanonical, canonical, and isobaric-isothermal thermodynamic ensembles. In addition, we report the expressions for covalently bonded QM-MM frontiers using the link atom approach.

We implemented the PBC QM/MM analytic gradients and validated them through several MD equilibrations for different test systems. Overall, we show that the NVE dynamics conserve the total energy even when using 1 femtosecond timesteps, despite a small drift of the total energy on longer timescales. In addition, we extracted free energy profiles for the isomerization of proline amino acid and proline peptide in water. We show that our QM/MM method leads to accurate isomerization barriers compared to experimental data, without manipulating the forcefield parameters.

Despite our implementation being efficient at computing the QM/MM interaction for large systems, the computation of free energy profiles is limited by the computational cost of the QM method, since it requires an extended phase-space sampling through MD at the nanosecond timescale. Accelerated sampling techniques and highly parallelized QM and MM codes will be required to apply this method for routine computations of free energy profiles.

Acknowledgement We acknowledge the support from "Agence Nationale de la Recherche" through the project MAPPLE (ANR-22-CE29-0014-01). Centre de Calcul Intensif d'Aix-Marseille is acknowledged for granting access to high-performance computing resources.

Supporting Information Available

Supporting information contains explicit derivations of the interaction energy, the derivatives of the electrostatic external potential, the derivatives with respect to link atoms, and the full expression of derivatives with respect to lattice parameters. This information is available free of charge via the Internet at http://pubs.acs.org.

References

(1) Warshel, A.; Levitt, M. Theoretical studies of enzyme reactions: dielectric, electrostatic and steric stabilisation of the carbonium ion in the reaction of lysozyme. *J. Mol. Biol.* **1976**, *103*, 227–249.

(2) Senn, H. M.; Thiel, W. QM/MM Methods for Biomolecular Systems. *Angew. Chem., Int. Ed.* **2009**, *48*, 1198–1229.

(3) Warshel, A.; Russell, S. T. Calculations of electrostatic interactions in biological systems and in solutions. *Q. Rev. Biophys.* **1984**, *17*, 283–422.

(4) Honig, B.; Nicholls, A. Classical Electrostatics in Biology and Chemistry. *Science* **1995**, *268*, 1144–1149.

(5) Nakamura, H. Roles of electrostatic interaction in proteins. *Q. Rev. Biophys.* **1996**, *29*, 1–90.

(6) Brooks, C. L.; Pettitt, B. M.; Karplus, M. Structural and energetic effects of truncating long ranged interactions in ionic and polar fluids. *J. Chem. Phys.* **1985**, *83*, 11.

(7) Steinbach, P. J.; Brooks, B. R. New Spherical-Cutoff Methods for Long-Range Forces in Macromolecular Simulation. *J. Comp. Chem.* **1994**, *15*, 667–683.

(8) Schreiber, H.; Steinhauser, O. Cutoff Size Does Strongly Influence Molecular Dynamics Results on Solvated Polypeptides. *Biochem.* **1992**, *31*, 5856–5860.

(9) Schreiber, H.; Steinhauser, O. Molecular dynamics studies of solvated polypeptides: why the cut-off scheme does not work. *Chem. Phys.* **1992**, *168*, 75–89.

(10) York, D. M.; Darden, T. A.; Pedersen, L. G. The effect of longrange electrostatic interactions in simulations of macromolecular crystals: A comparison of the Ewald and truncated list methods. *J. Chem. Phys.* **1993**, *99*, 8345.

(11) York, D. M.; Yang, W.; Lee, H.; Darden, T.; Pedersen, L. G. Toward the Accurate Modeling of DNA: The Importance of Long-Range Electrostatics. *J. Am. Chem. Soc.* **1995**, *117*, 5001–5002.

(12) Feller, S. E.; Pastor, R. W.; Rojnuckarin, A.; Bogusz, S.; Brooks, B. R. Effect of Electrostatic Force Truncation on Interfacial and Transport Properties of Water. *J. Phys. Chem.* **1996**, *100*, 17011–17020.

(13) Mathias, G.; Egwolf, B.; Nonella, M.; Tavan, P. A fast multipole method combined with a reaction field for long-range electrostatics in molecular dynamics simulations: The effects of truncation on the properties of water. *J. Chem. Phys.* **2003**, *118*, 10847.

(14) Patra, M.; Karttunen, M.; Hyvönen, M. T.; Falck, E.; Lindqvist, P.; Vattulainen, P. Molecular Dynamics Simulations of Lipid Bilayers: Major Artifacts Due to Truncating Electrostatic Interactions. *Biophys. J.* **2003**, *84*, 3636–3645.

(15) Schaefer, P.; Riccardi, D.; Cui, Q. Reliable treatment of electrostatics in combined QM/MM simulation of macromolecules. *J. Chem. Phys.* **2005**, *123*, 014905.

(16) Wolf, D.; Keblinski, P.; Phillpot, S. R.; Eggebrecht, J. Exact method for the simulation of Coulombic systems by spherically truncated, pairwise r-1 summation. *J. Chem. Phys.* **1999**, *110*, 8254.

(17) Zahn, D.; Schilling, B.; Kast, S. M. Enhancement of the Wolf Damped Coulomb Potential: Static, Dynamic, and Dielectric Properties of Liquid Water from Molecular Simulation. *J. Phys. Chem. B* **2002**, *106*, 10725–10732.

(18) Fennell, C. J.; Gezelter, J. D. Is the Ewald summation still necessary? Pairwise alternatives to the accepted standard for long-range electrostatics. *J. Chem. Phys.* **2006**, *124*, 234104.

(19) McCann, B. W.; Acevedo, O. Pairwise Alternatives to Ewald Summation for Calculating Long- Range Electrostatics in Ionic Liquids. *J. Chem. Theory Comput.* **2013**, *9*, 944–950.

(20) Wu, X.; Brooks, B. R. Isotropic periodic sum: A method for the calculation of long- range interactions. *J. Chem. Phys.* **2005**, *122*, 44107.

(21) Wu, X.; Brooks, B. R. Isotropic periodic sum of electrostatic interactions for polar systems. *J. Chem. Phys.* **2009**, *131*, 024107.

(22) Ojeda-May, P.; Pu, J. Isotropic Periodic Sum Treatment of Long-Range Electrostatic Interactions in Combined Quantum Mechanical and Molecular Mechanical Calculations. *J. Chem. Theory Comput.* **2014**, *10*, 134–145.

(23) Takahashi, K. Z.; Narumi, T.; Suh, D.; Yasuoka, K. An Improved Isotropic Periodic Sum Method That Uses Linear Combinations of Basis Potentials. *J. Chem. Theory Comput.* **2012**, *8*, 4503–4516.

(24) Fukuda, I.; Yonezawa, Y.; Nakamura, H. Molecular dynamics scheme for precise estimation of electrostatic interaction

via zero-dipole summation principle. *J. Chem. Phys.* **2011**, *134*, 164107.

(25) Pan, X.; Nam, K.; Epifanovsky, E.; Simmonett, A. C.; Rosta, E.; Shao, Y. A simplified charge projection scheme fir long-range electrostatics in ab initio QM/MM calculations. *J. Chem. Phys.* **2021**, *154*, 024115.

(26) L. Greengard, L.; Rokhlin, V. Fast Algorithm for Particle Simulations. *J. Comput. Phys.* **1987**, *73*, 315–348.

(27) Pollock, E. L.; Glosli, J. Comments on P3M, FMM, and the Ewald method for large periodic Coulombic systems. *Comput. Phys. Comm.* **1996**, *95*, 93–110.

(28) Kurzak, J.; Pettitt, B. M. Fast multipole methods for particle dynamics. *Mol. Simul.* **2006**, *32*, 775–790.

(29) Ewald, P. P. Die Berechnung optischer und elektrostatischer Gitterpotentiale. *Ann. Phys.* **1921**, *369*, 253–287.

(30) Hockney, R. W.; Eastwood, J. W. *Computer Simulation Using Particles*; Taylor & Francis, 1988.

(31) Toukmaji, A. Y.; Board Jr., J. A. Ewald summation techniques in perspective: a survey. *Comput. Phys. Commun.* **1996**, *95*, 73–92.

(32) Darden, T.; York, D.; Pedersen, L. Particle mesh Ewald: An N·log(N) method for Ewald sums in large systems. *J. Chem. Phys.* **1993**, *98*, 10089–10092.

(33) Essmann, U.; Perera, L.; Berkowitz,; Max L., T., Darden; Lee, H.; Pedersen, L. G. A smooth particle mesh Ewald method. *J. Chem. Phys.* **1995**, *103*, 8577–8593.

(34) York, D. M.; Yang, W. The fast Fourier Poisson method for calculating Ewald sums. *J. Chem. Phys.* **1994**, *101*, 3298.

(35) Sagui, C.; Darden, T. A. Molecular Dynamics Simulations of Biomolecules: Long-Range Electrostatic Effects. *Annu. Rev. Bioph. Biom.* **1999**, *28*, 155–179.

(36) Cisneros, G. A.; Karttunen, M.; Ren, P.; Sagui, C. Classical Electrostatics for Biomolecular Simulations. *Chem. Rev.* **2014**, *114*, 779–814.

(37) Berkowitz, M.; McCammon, J. A. Molecular Dynamics with Stochastic Boundary Conditions. *Chem. Phys. Lett.* **1982**, *90*, 215–217.

(38) Lee, F. S.; Warshel, A. A local reaction field method for fast evaluation of longrange electrostatic interactions in molecular simulations. *J. Chem. Phys.* **1992**, *97*, 3100.

(39) Wang, L.; Hermans, J. Reaction Field Molecular Dynamics Simulation with Friedman's Image Charge Method. *J. Phys. Chem.* **1995**, *99*, 12001–12007.

(40) König, P. H.; Ghosh, N.; Hoffmann, M.; Elstner, M.; Tajkhorshid, E.; Frauenheim, T.; Cui, Q. Toward Theoretical Analyis of Long-Range Proton Transfer Kinetics in Biomolecular Pumps. *J. Phys. Chem.* **2006**, *110*, 548–563.

(41) Roux, B.; Simonson, T. Implicit solvent models. *Biophys. Chem.* **1999**, *78*, 1–20.

(42) Tomasi, J.; Mennucci, B.; Cammi, R. Quantum Mechanical Continuum Solvation Models. *Chem. Rev.* **2005**, *105*, 2999–3093.

(43) Nam, K.; Gao, J.; York, D. M. An Efficient Linear-Scaling Ewald Method for Long-Range Electrostatic Interactions in Combined QM/MM Calculations. *J. Chem. Theory Comput.* **2005**, *1*, 2–13.

(44) Riccardi, D.; Shaefer, P.; Cui, Q. pKa Calculations in Solution and Proteins with QM/MM Free Energy Perturbation Simulations: A Quantitative Test of

QM/MM Protocols. *J. Phys. Chem. B* **2005**, *109*, 17715–17733.

(45) Seabra, G. d. M.; Walker, R. C.; Elstner, M.; Case, D. A.; Roitberg, A. E. Implementation of the SCC-DFTB Method for Hybrid QM/MM Simulations within the Amber Molecular Dynamics Package. *J. Phys. Chem. A* **2007**, *111*, 5655–5664.

(46) Walker, R. C.; Crowley, M. F.; Case, D. A. The Implementation of a Fast and Accurate QM/MM Potential Method in Amber. *J. Comp. Chem.* **2008**, *29*, 1019–1031.

(47) Nam, K. Acceleration of Ab Initio QM/MM Calculations under Periodic Boundary Conditions by Multiscale and Multiple Time Step Approaches. *J. Chem. Theory Comput.* **2014**, *10*, 4175–4183.

(48) Nishizawa, H.; Okumura, H. Rapid QM/MM approach for biomolecular systems under periodic boundary conditions: Combination of the density-functional tight-binding theory and particle mesh Ewald method. *J. Comp. Chem.* **2016**, *37*, 2701–2711.

(49) Vasilevskaya, T.; Thiel, W. Periodic Boundary Conditions in QM/MM Calculations: Implementation and Tests. *J. Chem. Theory Comput.* **2016**, *12*, 3561–3570.

(50) Laino, T.; Mohamed, F.; Laio, A.; Parrinello, M. An Efficient Real Space Multigrid QM/MM Electrostatic Coupling. *J. Chem. Theory Comput.* **2005**, *1*, 1176–1184.

(51) Laino, T.; Mohamed, F.; Laio, A.; Parrinello, M. An Efficient Linear-Scaling Electrostatic Coupling for Treating Periodic Boundary Conditions in QM/MM Simulations. *J. Chem. Theory Comput.* **2006**, *2*, 1370–1378.

(52) Sanz-Navarro, C. F.; Grima, R.; García, A.; Bea, E. A.; Soba, A.; Cela, J. M.; Ordejón, P. An efficient implementation of a QM—MM method in SIESTA. *Theor. Chem. Acc.* **2011**, *128*, 825–833.

(53) Holden, Z. C.; Richard, R. M.; Herbert, J. M. Periodic boundary conditions for QM/MM calculations: Ewald summation for extended Gaussian basis sets. *J. Chem. Phys.* **2013**, *139*, 244108.

(54) Holden, Z. C.; Richard, R. M.; Herbert, J. M. Erratum: "Periodic boundary conditions for QM/MM calculations: Ewald summation for extended Gaussian basis sets" [J. Chem. Phys. 139, 244108 (2013)]. *J. Chem. Phys.* **2015**, *142*, 059901.

(55) Torras, J. Multiple active zones in hybrid QM/MM molecular dynamics simulations for large biomolecular systems. *Phys. Chem. Chem. Phys.* **2015**, *17*, 9959–9972.

(56) Giese, T. J.; York, D. M. Ambient-Potential Composite Ewald Method for ab Initio Quantum Mechanical/Molecular Mechanical Molecular Dynamics Simulation. *J. Chem. Theory Comput.* **2016**, *12*, 2611–2632.

(57) Holden, Z. C.; Rana, B.; Herbert, J. M. Analytic gradient for the QM/MM-Ewald method using charges derived from the electrostatic potential: Theory, implementation, and application to ab initio molecular dynamics simulation of the aqueous electron. *J. Chem. Phys.* **2019**, *150*, 144115.

(58) Kawashima, Y.; Ishimura, K.; Shiga, M. Ab initio quantum mechanics/molecular mechanics method with periodic boundaries employing Ewald summation technique to electron-charge interaction: Treatment of the surface-dipole term. *J. Chem. Phys.* **2019**, *150*, 124103.

(59) Pederson, J. P.; McDaniel, J. G. DFT-based QM/MM with particle-mesh

Ewald for direct, long-range electrostatic embedding. *J. Chem. Phys.* **2022**, *156*, 174105.

(60) Bonfrate, S.; Ferré, N.; Miquel,; Huix-Rotllant, An efficient electrostatic embedding QM/MM method using periodic boundary conditions based on particle-mesh Ewald sums and electrostatic potential fitted charge operators. *J. Chem. Phys.* **2023**, *158*, 021101.

(61) Ferré, N.; Ángyán, J. G. Approximate electrostatic interaction operator for QM/MM calculations. *Chem. Phys. Lett.* **2002**, *356*, 331–339.

(62) Huix-Rotllant, M.; Ferré, N. Analytic Energy, Gradient, and Hessian of Electrostatic Embedding QM/MM Based on Electrostatic Potential-Fitted Atomic Charges Scaling Linearly with the MM Subsystem Size. *J. Chem. Theory Comput.* **2021**, *17*, 538–548.

(63) Pulay, P. Analytical derivatives, forces, force constants, molecular geometries, and related response properties in electronic structure theory. *Wiley Interdiscip. Rev. Comput. Mol. Sci.* **2014**, *4*, 169–181.

(64) Tsai, D. H. The virial theorem and stress calculation in molecular dynamics. *J. Chem. Phys.* **1979**, *70*, 1375–1382.

(65) Schwinn, K.; Ferré, N.; Huix-Rotllant, M. Analytic QM/MM atomic charge derivatives avoiding the scaling of coupled perturbed equations with the MM subsystem size. *J. Chem. Phys.* **2019**, *151*, 041102.

(66) Pople, J. A.; Krishnan, R.; Schlegel, H. B.; Binkley, J. S. Derivative studies in Hartree-Fock and Møller-Plesset theories. *Int. J. Quantum Chem.* **1979**, *16*, 225–241.

(67) Assfeld , X.; Rivail, J.-L. Quantum chemical computations on parts of large molecules: the ab initio local self consistent field method. *Chem. Phys. Lett.* **1996**, *263*, 100–106.

(68) Gao, J.; Amara, P.; Alhambra, C.; Field, M. J. A Generalized Hybrid Orbital (GHO) Method for the Treatment of Boundary Atoms in Combined QM/MM Calculations. *J. Phys. Chem. A* **1998**, *102*, 4714–4721.

(69) Antes , I.; Thiel, W. Adjusted connection atoms for combined quantum mechanical and molecular mechanical methods. *J. Phys. Chem. A* **1999**, *103*, 9290–9295.

(70) Das, D.; Eurenius, K. P.; Billings, E. M.; Sherwood, P.; Chatfield, D. C.; Hodošček, M.; Brooks, B. R. Optimization of quantum mechanical molecular mechanical partitioning schemes: Gaussian delocalization of molecular mechanical charges and the double link atom method. *J. Chem. Phys.* **2002**, *117*, 10534–10547.

(71) Di Labio, G. A.; Hurley, M. M.; Christiansen, P. A. Simple one-electron quantum capping potentials for use in hybrid QM/MM studies of biological molecules. *J. Chem. Phys.* **2002**, *116*, 9578–9584.

(72) Ferré, N.; Assfeld, X.; Rivail, J.-L. Specific force field parameters determination for the hybrid *ab initio* QM/MM LSCF method. *J. Comp. Chem.* **2002**, *23*, 610–624.

(73) Swart, M. AddRemove: A new link model for use in QM/MM studies. *I. J. Quant. Chem.* **2003**, *91*, 177–183.

(74) Amara , P.; Field, M. J. Evaluation of an ab initio quantum mechanical/molecular mechanical hybrid-potential link-atom method. *Theor. Chem. Acc.* **2003**, *109*, 43–52.

(75) Ferré , N.; Olivucci, M. The peptide bond: pitfalls and drawbacks of the link atom scheme. *J. Molec. Struct. (Theochem)* **2003**, *632*, 71–82.

(76) Ferré, N.; Cembran, A.; Garavelli, M.; Olivucci, M. Complete-active-space self-consistent-field/Amber parameterization of the Lys296-Retinal-Glu113 rhodopsin chromophore-counterion system. *Theor. Chem. Acc.* **2004**, *112*, 335–341.

(77) Lin , H.; Truhlar, D. G. Redistributed Charge and Dipole Schemes for Combined Quantum Mechanical and Molecular Mechanical Calculations. *J. Phys. Chem. A* **2005**, *109*, 3991–4004.

(78) von Lilienfeld , O. A.; Tavernelli, I.; Rothlisberger, U. Variational optimization of effective atom centered potentials for molecular properties. *J. Chem. Phys.* **2005**, *122*, 014113–1–6.

(79) Fornili, A.; Loos, P.-F.; Sironi, M.; Assfeld, X. Frozen core orbitals as an alternative to specific frontier bond potential in hybrid Quantum Mechanics/Molecular Mechanics methods. *Chem. Phys. Lett.* **2006**, *427*, 236–240.

(80) Vreven, T.; Byun, K. S.; Komaromi, I.; Dapprich, S.; Montgomery Jr., J. A.; Morokuma, K.; Frisch, M. J. Combining Quantum Mechanics Methods with Molecular Mechanics Methods in ONIOM. *J. Chem. Theory Comput.* **2006**, *2*, 815–826.

(81) Loos , P.-F.; Assfeld, X. Self-Consistent Strictly Localized Orbitals. *J. Chem. Theor. Comput.* **2007**, *3*, 1047–1053.

(82) Wang , B.; Truhlar, D. G. Combined Quantum Mechanical and Molecular Mechanical Methods for Calculating Potential Energy Surfaces: Tuned and Balanced Redistributed-Charge Algorithm. *J. Chem. Theory Comput.* **2010**, *6*, 359–369.

(83) Chaudret, R.; Parks, J. M.; Yang, W. Pseudobond parameters for QM/MM studies involving nucleosides, nucleotides, and their analogs. *J. Chem. Phys.* **2013**, *138*, 045102.

(84) Monari, A.; Rivail, J.-L.; Assfeld, X. Theoretical Modeling of Large Molecular Systems. Advances in the Local Self Consistent Field Method for Mixed Quantum Mechanics/Molecular Mechanics Calculations. *Acc. Chem. Res.* **2013**, *46*, 596–603.

(85) Hitzenberger, M.; Ratanasak, M.; Parasuk, V.; Hofer, T. S. Optimizing link atom parameters for DNA QM/MM simulations. *Theor. Chem. Acc.* **2016**, *135*.

(86) Singh, U. C.; Kollman, P. A. A combined ab initio quantum mechanical and molecular mechanical method for carrying out simulations on complex molecular systems: Applications to the CH3Cl + Cl- exchange reaction and gas phase protonation of polyethers. *J. Comput. Chem.* **1986**, *7*, 718–730.

(87) Field , M. J.; Bash, P. A.; Karplus, M. A combined quantum mechanical and molecular mechanical potential for molecular dynamics simulations. *J. Comput. Chem.* **1990**, *11*, 700–733.

(88) Maseras , F.; Morokuma, K. IMOMM: A new integrated ab initio + molecular mechanics geometry optimization scheme of equilibrium structures and transition states. *J. Comput. Chem.* **1995**, *16*, 1170–1179.

(89) Dapprich, S.; Komáromi, I.; Suzie Byun, K.; Morokuma, K.; Frisch, M. J. A new ONIOM implementation in Gaussian98. Part I. The calculation of energies, gradients, vibrational frequencies and electric field derivatives. *J. Molec. Struct. (Theochem)* **1999**, *461-462*, 1–21.

(90) Torrie, G. M.; Valleau, J. P. Nonphysical sampling distributions in Monte Carlo free-energy estimation: Umbrella sampling. *Journal of Computational Physics* **1977**, *23*, 187–199.

(91) Kumar, S.; Rosenberg, J. M.; Bouzida, D.; Swendsen, R. H.; Kollman, P. A. The weighted histogram analysis method for free-energy calculations on biomolecules. I. The method. *J. Comp. Chem.* **1992**, *13*, 1011–1021.

(92) Grossfield, A. WHAM: the weighted histogram analysis method, version 2.0.11. 2023; `http://membrane.urmc.rochester.edu/content/wham`, accessed 2023-11-23.

(93) Pettersen, E. F.; Goddard, T. D.; Huang, C. C.; Meng, E. C.; Couch, G. S.; Croll, T. I.; Morris, J. H.; Ferrin, T. E. UCSF ChimeraX: Structure visualization for researchers, educators, and developers. *Protein Sci.* **2021**, *30*, 70–82.

(94) Rassolov, V. A.; Pople, J. A.; Ratner, M. A.; Windus, T. L. 6-31G* basis set for atoms K through Zn. *J. Chem. Phys.* **1998**, *109*, 1223–1229.

(95) MacKerell, A. D. J.; Bashford, D.; Bellott, M.; Dunbrack, R. L. J.; Evanseck, J. D.; Field, M. J.; Fischer, S.; Gao, J.; Guo, H.; Ha, S.; Joseph-McCarthy, D.; Kuchnir, L.; Kuczera, K.; Lau, F. T. K.; Mattos, C.; Michnick, S.; Ngo, T.; Nguyen, D. T.; Prodhom, B.; Reiher, W. E.; Roux, B.; Schlenkrich, M.; Smith, J. C.; Stote, R.; Straub, J.; Watanabe, M.; Wiórkiewicz-Kuczera, J.; Yin, D.; Karplus, M. All-Atom Empirical Potential for Molecular Modeling and Dynamics Studies of Proteins. *J. Phys. Chem. B* **1998**, *102*, 3586–3616.

(96) Melaccio, F.; Olivucci, M.; Lindh, R.; Ferré, N. Unique QM/MM potential energy surface exploration using microiterations. *Int. J. Quantum Chem.* **2011**, *111*, 3339–3346.

(97) Allen, M. P.; Tildesley, D. J. *Computer Simulation of Liquids*; Oxford University Press, 2017.

(98) Eastman, P.; Pande, V. S. Energy Conservation as a Measure of Simulation Accuracy. *bioRxiv* **2016**,

(99) Marx, D.; Hutter, J. *Ab Initio Molecular Dynamics: Basic Theory and Advanced Methods*; Cambridge University Press, 2009.

(100) Schmid, F. X.; Mayr, L. M.; Mucke, M.; Schonbrunner, E. R. Prolyl Isomerases: Role in Protein Folding. *Adv. Protein Chem.* **1993**, *44*, 25–66.

(101) Stein, R. L. Mechanism of Enzymatic and Nonenzymatic Prolyl Cis-Trans Isomerization. *Adv. Protein Chem.* **1993**, *44*, 1–24.

(102) Fischer, G.; Bang, H.; Mech, C. Nachweis einer Enzymkatalyse für die cis-trans-Isomerisierung der Peptidbindung in prolinhaltigen Peptiden. *Biomed. Biochim. Acta* **1984**, *43*, 1101–1111.

(103) Hamelberg, D.; McCammon, J. A. Mechanistic Insight into the Role of Transition-State Stabilization in Cyclophilin A. *J. Am. Chem. Soc.* **2009**, *131*, 147–152.

(104) Beausoleil, E.; Lubell, W. D. Steric Effects on the Amide Isomer Equilibrium of Prolyl Peptides. Synthesis and Conformational Analysis of N-Acetyl-5-tert-butylproline N'-Methylamides. *J. Am. Chem. Soc.* **1996**, *118*, 12902–12908.

(105) Kang, Y. K.; Jhon, J. S.; Han, S. J. Conformational study of Ac-Xaa-Pro-NHMe dipeptides: proline puckering and trans/cis imide bond. *J. Pept. Res.* **1999**, *53*, 30–40.

(106) Hur, S.; Bruice, T. C. The Mechanism of Cis-Trans Isomerization of Prolyl Peptides by Cyclophilin. *J. Am. Chem. Soc.* **2002**, *124*, 7303–7313.

(107) Agarwal, P. K.; Geist, A.; Gorin, A. Protein Dynamics and Enzymatic Catalysis: Investigating the Peptidyl-Prolyl

Cis-Trans Isomerization Activity of Cyclophilin A. *Biochemistry* **2004**, *43*, 10605–10618.

(108) Kang, Y. K. Ab initio and DFT conformational study of proline dipeptide. *J. Mol. Struct. THEOCHEM* **2004**, *675*, 37–45.

(109) Di Martino, G. P.; Masetti, M.; Cavalli, A.; Recanatini, M. Mechanistic insights into Pin1 peptidyl-prolyl cis-trans isomerization from umbrella sampling simulations. *Proteins* **2014**, *82*, 2943–2956.

(110) Wapeesittipan, P.; Mey, A. S. J. S.; Walkinshaw, M. D.; Michel, J. Allosteric effects in cyclophilin mutants may be explained by changes in nano-microsecond time scale motions. *Comm. Chem.* **2019**, *2*.

(111) Jorgensen, W. L.; Chandrasekhar, J.; Madura, J. D.; Impey, R. W.; Klein, M. L. Comparison of simple potential functions for simulating liquid water. *J. Chem. Phys.* **1983**, *79*, 926.

(112) Binkley, J. S.; Pople, J. A.; Hehre, W. J. Self-consistent molecular orbital methods. 21. Small split-valence basis sets for first-row elements. *J. Am. Chem. Soc.* **1980**, *102*, 939–947.

(113) Wang, J.; Cieplak, P.; Kollman, P. A. How well does a restrained electrostatic potential (RESP) model perform in calculating conformational energies of organic and biological molecules? *J. Comput. Chem.* **2000**, *21*, 1049–1074.

(114) Hornak, V.; Abel, R.; Okur, A.; Strockbine, B.; Roitberg, A.; Simmerling, C. Comparison of multiple Amber force fields and development of improved protein backbone parameters. *Proteins* **2006**, *65*, 712–725.

(115) Doshi, U.; Hamelberg, D. Reoptimization of the AMBER Force Field Parameters for Peptide Bond (Omega) Torsions Using Accelerated Molecular Dynamics. *J. Phys. Chem. B* **2009**, *113*, 16590–16595.

(116) Brémond, E.; Savarese, M.; Rega, N.; Ciofini, I.; Adamo, C. Free Energy Profiles of Proton Transfer Reactions: Density Functional Benchmark from Biased Ab Initio Dynamics. *J. Chem. Theory Comput.* **2022**, *18*, 1501–1511.

(117) Shukla, P. B.; Mishra, P.; Baruah, T.; Zope, R. R.; Jackson, K. A.; Johnson, J. K. How Do Self-Interaction Errors Associated with Stretched Bonds Affect Barrier Height Predictions? *J. Phys. Chem. A* **2023**, *127*, 1750–1759.

(118) Wang, J.; Wolf, R. M.; Caldwell, J. W.; Kollman, P. A.; Case, D. A. Development and testing of a general AMBER force field. *J. Comp. Chem.* **2004**, *25*, 1157–1174.

(119) Zlobin, A.; Belyaeva, J.; Golovin, A. Challenges in Protein QM/MM Simulations with Intra-Backbone Link Atoms. *J. Chem. Inf. Model.* **2023**, *63*, 546–560.

(120) Harrison, R. K.; Stein, R. L. Mechanistic studies of enzymic and nonenzymic prolyl cis-trans isomerization. *J. Am. Chem. Soc.* **1992**, *114*, 3464–3471.

TOC Graphic

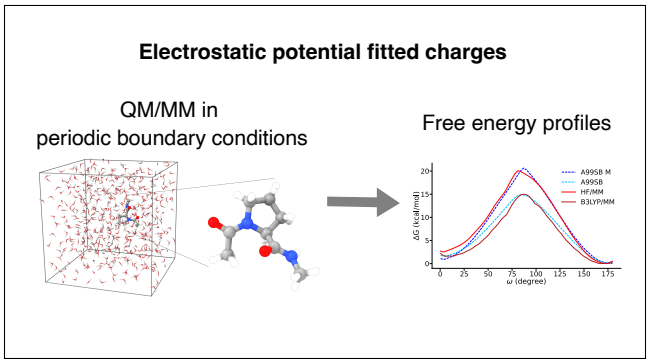
Electrostatic potential fitted charges
QM/MM in
periodic boundary conditions
Free energy profiles
A99SB M
A99SB
HF/MM
B3LYP/MM
ΔG (kcal/mol)
ω (degree)